

# Particle-hole asymmetry on Hall conductivity of a topological insulator

Zhou Li<sup>1\*</sup> and J. P. Carbotte<sup>1,2†</sup>

<sup>1</sup> *Department of Physics, McMaster University, Hamilton, Ontario, Canada, L8S 4M1*

<sup>2</sup> *Canadian Institute for Advanced Research, Toronto, Ontario, Canada M5G 1Z8*

(Dated: October 31, 2018)

The helical Dirac states on the surface of a topological insulator are protected by topology and display significant particle-hole asymmetry. This asymmetry arises from a subdominant Schrödinger type contribution to the Hamiltonian which provides a small perturbation to a dominant Dirac contribution. This changes the Landau levels energies in an external magnetic field ( $B$ ) and provides modifications to the usual relativistic optical matrix elements. Nevertheless we find that the relativistic quantization of the Hall plateaux remains even when the ratio of the Schrödinger ( $E_0$ ) to Dirac ( $E_1$ ) magnetic energy scale increases either through an increase in  $B$ , a decrease in the Schrödinger mass or of the Dirac fermi velocity. First corrections to the optical matrix elements (OME) in the relativistic case drop out at least to order  $(E_0/E_1)^3$ . In the opposite limit  $E_1$  small, the quantization remains classical but there is a split into two series. The first corrections to the OME in this case, cancel out at least to order  $(E_1/E_0)^4$ .

PACS numbers: 73.43.Cd, 71.70.Di, 73.25.+i

## I. INTRODUCTION

In graphene, the Dirac cones associated with conduction and valence bands are normally taken to have perfect particle-hole symmetry about the Dirac point. On the other hand the topologically protected helical Dirac fermions on the metallic surface<sup>1,2</sup> of a topological insulator (TI) also show Dirac dispersion<sup>3-6</sup> curves with spin momentum locking, but they generally display significant particle-hole asymmetry<sup>3-10</sup>. This leads to electronic dispersion curves characterized by an hourglass or goblet shape with valence band below the Dirac point fanning out more rapidly than the corresponding conduction band. Its wider base eventually merges with the bulk valence band at which point it no longer can be traced as a separated entity. This behavior is modeled by including, in addition to a dominant Dirac linear in momentum piece, a subdominant Schrödinger contribution quadratic in momentum with mass  $m$ . This term leads directly to the restructuring of the perfect Dirac dispersions to goblet dispersions instead.

Even a small Schrödinger term in the Hamiltonian can have important consequences for the properties of topological insulators. As an example, Wright and McKenzie<sup>11-13</sup> have very recently found for gapped systems that a finite  $m$  term can lead to important changes in the phase of the quantum oscillations associated with Shubrikov-de-Hass or de-Hass-van Alphen effects.<sup>14-20</sup> The phase offset ( $\gamma$ ) of these oscillations is determined not only by the Berry phase of the cyclotron orbits involved, but by a further amount which exists only when the Schrödinger term is present i.e.  $m \neq \infty$ .<sup>11-13</sup> As a second example, the magneto optical absorption lines of a TI<sup>9</sup> split into two peaks in contrast to the single peak of graphene because of the particle-hole asymmetry. The interband transitions allowed by the optical selection rules from Landau level (LL)  $-n$  in the valence band to  $n+1$  in the conduction band and from  $-(n+1)$  to  $n$  are no longer

degenerate in energy as they would be in graphene.<sup>21-23</sup>

In graphene the electron dynamics is determined by the relativistic Dirac equation and the integer quantum Hall effect is unconventional.<sup>24-29</sup> The DC Hall conductivity has plateaux in units of  $2e^2/h$  at  $(2n+1)$  with  $n = 0, 1, 2, 3, \dots$  which is to be contrasted with the conventional case of Schrödinger dynamics where quantization is  $2n$  rather than  $(2n+1)$ . An important question which we wish to address in this paper is how does a small subdominant Schrödinger piece in the Hamiltonian change the Dirac sequence of the dominant Dirac piece. Even without such a complication we know that impurity scattering and/or temperature affects the integrity of the Hall plateaux eventually smearing them out towards the classical unquantized result.<sup>25,26</sup>

The paper is structured as follows. The formalism associated with the Landau levels (LL) created by an external magnetic field ( $B$ ) oriented perpendicular to the surface of the topological insulator is presented in section II. Eigen energies and wave functions are written in terms of the Schrödinger  $E_0 = \hbar e|B|/m$  and Dirac  $E_1 = \hbar v_F \sqrt{e|B|/\hbar}$  magnetic energies with  $v_F$  the Dirac velocity. The general formula for the Hall conductivity is specified, and its DC limit is taken. In section III the resulting formula is shown to reduce to the known Schrödinger and Dirac quantization  $0, 1, 2, 3, \dots$  and  $1/2, 3/2, 5/2, \dots$  respectively when there is only a quadratic or linear in momentum term in the Hamiltonian. For graphene we have a factor of 4 from spin and valley degeneracy not included here. In the more general case when both terms are present the resulting expressions are complicated. In section IV, expanding OME in powers of  $E_0/E_1$ , we show that the resulting simplified equation that determines the Hall plateaux has the same form as for pure Dirac but with the new Landau level (LL) energies appropriate to the TI. All corrections from OME have dropped out at least to order cubic in the ratio  $E_0/E_1$ . We also consider the opposite limit appropriate

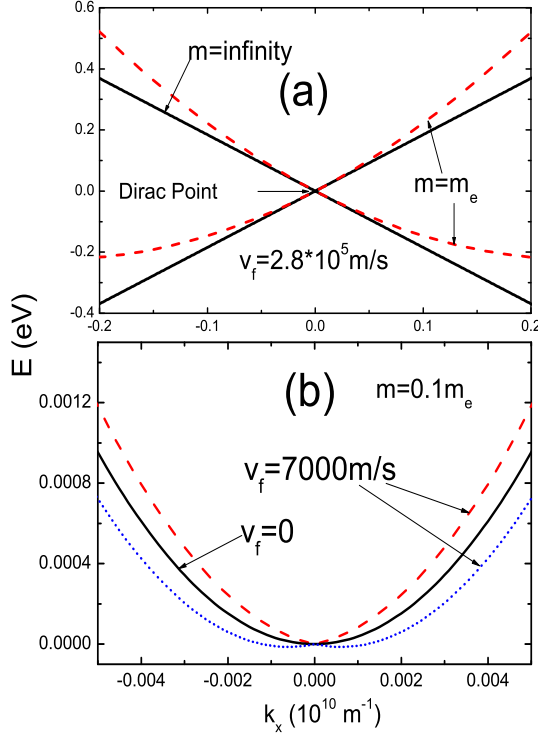


FIG. 1. (Color online) a) Solid curves (black) give the perfect Dirac cones when the Schrödinger piece in Eq. (1) is ignored. These are shown for comparison with the dashed curve (red) which includes both Schrödinger and Dirac contribution (topological insulators). b) Solid curve (black) gives the perfect Schrödinger dispersion when the Dirac piece in Eq. (1) is ignored. This is shown for comparison with the dashed red and dotted blue curves which include both Schrödinger and Dirac contribution (spintronic semiconductors).

to present day spintronic semiconductors for which the Schrödinger term is dominant but a small Dirac contribution is also present. Expanding the OME in powers of  $E_1/E_0$  we find that they cancel out at least to order  $(E_1/E_0)^4$  and the equations reduce to the pure classical equations but with the new LL energies, and two such series are involved. In the same section we present numerical results. Details of the derivations are to be found in an appendix. A summary and conclusions make up section V.

## II. FORMALISM

A minimal Hamiltonian for describing the helical Dirac fermions that exist at the surface of a three dimensional topological insulator has the form

$$H_0 = \frac{\hbar^2 k^2}{2m} + \hbar v_F (k_x \sigma_y - k_y \sigma_x) \quad (1)$$

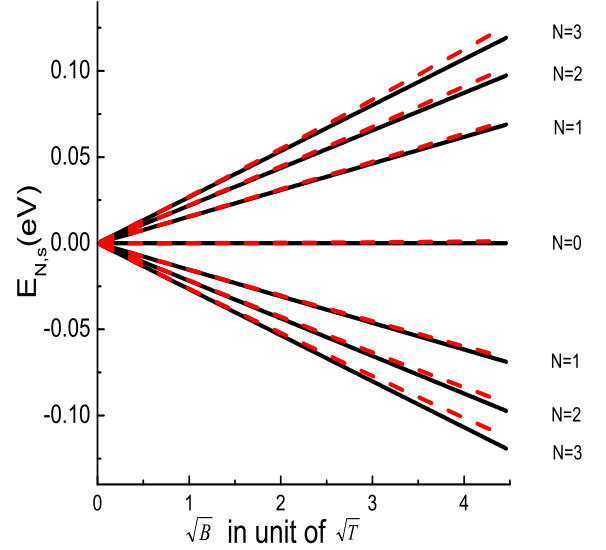


FIG. 2. (Color online) Landau level energies  $E_{N,s}$  labeled by the index  $N$  as a function of the square root of the magnetic field  $B$  measured in Tesla for the same band structure parameters as in Fig. 1(a). Solid (black) straight lines are for comparison and represent the pure Dirac case for which  $m = \infty$  in Eq. (1). The dashed (red) lines include a small Schrödinger contribution. This can have a strong effect, particularly on the negative energy state with large value of  $N$  (LL index).

where  $\sigma_x, \sigma_y$  are the spin Pauli matrices and  $\mathbf{k}$  is momentum. The first term is the usual quadratic in momentum Schrödinger contribution with effective mass  $m$  and the second describes Dirac fermions with velocity  $v_F$ . The dispersion curves associated with Eq. (1) are

$$\varepsilon_{k,\pm} = \frac{\hbar^2 k^2}{2m} \pm \hbar v_F k \quad (2)$$

These are displayed in Fig. 1a for a set of parameters typical for topological insulators namely  $v_F = 2.8 * 10^5 m/s$  and  $m$  equal to the bare electron mass ( $m_e$ ). For reference, in the specific case of  $Bi_2Te_3$ ,  $v_F = 4.3 * 10^5 m/s$  and  $m = 0.09 m_e$ . The solid (black) curves in Fig. 1a are for pure Dirac and are included for comparison with dashed (red) curves which give the electron dispersion  $\varepsilon_{k,\pm}$  of Eq. (2) when  $m = m_e$ . This piece adds on to the black curves in both conduction and valence band and leads to a goblet or hourglass shape. It narrows the cone cross-section as energy is increased in the conduction band while it widens that in the valence band with decreasing energy below the Dirac point at  $E = 0$ . The particle-hole asymmetry displayed in Fig. 1a can be characterized by the value of momentum  $k_c$  at which the valence band has a minimum value. We find  $k_c = v_F m / \hbar \simeq .58 \text{ \AA}^{-1}$  and the energy at minimum is  $\frac{\hbar^2 k_c^2}{2m} - \hbar v_F k_c = -\frac{1}{2} m v_F^2 \simeq -220 meV$ . For the parameters estimated from first principle calculations in  $Bi_2Te_3$

this minimum energy would be much smaller of order  $48\text{meV}$ . In Fig. 1b we show the same dispersion curves but for a very different set of parameters which are more representative of semiconductors presently used in spintronics. The Dirac fermi velocity is much smaller than that used in the top frame for topological insulators and the Schrödinger mass has also been taken to be a factor of 10 smaller. The solid black curve applies to the pure Schrödinger case and is for comparison. The red dashed and blue dotted curves include the small Dirac contribution.

Turning next to the effect on electron dynamics of a magnetic field  $B$  oriented perpendicular to the surface of the TI we replace Eq. (1) in the Landau gauge by

$$H_0 = \frac{\hbar^2[(-i\partial_x)^2 + (-i\partial_y + eBx/\hbar)^2]}{2m} + \alpha[(-i\partial_x)\sigma_y - (-i\partial_y + eBx/\hbar)\sigma_x] \quad (3)$$

where  $\alpha = \hbar v_F$ ,  $\mathbf{B} = B\hat{z}$  and  $\hat{z}$  is a unit vector perpendicular to the surface plane. The energies of the Landau levels (LL) ignoring Zeeman splitting are

$$E_{N,s} = \hbar^2 N / (ml_B^2) + s\sqrt{[\hbar^2 / (2ml_B^2)]^2 + 2N\alpha^2 / l_B^2} \quad (4)$$

where the magnetic coherence length  $l_B = 1/\sqrt{e|B|/\hbar}$  with  $e$  the electron charge,  $N \neq 0$  is the LL index and  $s = \pm$  gives conduction (+) and valence (-) band respectively. For  $N = 0$

$$E_{N=0} = \hbar^2 / (2ml_B^2) \quad (5)$$

The energy levels  $E_{N,s}$  as a function of the square root of the magnetic field  $B$  in Tesla are plotted in Fig. 2 for the illustrative parameters defined in Fig. 1a. It is convenient to define a Schrödinger magnetic energy scale as  $E_0 = \hbar e|B|/m$  (here  $E_0 \approx 0.116\text{ meV}$  for  $B = 1\text{ T}$ ) and an equivalent Dirac magnetic scale as  $E_1 = \alpha\sqrt{e|B|/\hbar}$  (here  $E_1 \approx 10.4\text{ meV}$  for  $B = 1\text{ T}$ ) and also introduce a Diracness ratio  $P \equiv E_1^2/E_0^2$ . In this case  $P \rightarrow \infty$  corresponds to pure Dirac and  $P \rightarrow 0$  to pure Schrödinger. The significance of this parameter is that we will seek corrections to pure Dirac in powers of  $1/P \equiv x$  with  $x \ll 1$  and pure Schrödinger in powers of  $P$  with  $P \ll 1$ . While we will show later that our theory does reduce to the well known integer quantum Hall effect seen in semiconductors, when we consider the limit  $P \rightarrow 0$ , for the main part we will be interested in small deviation from a pure Dirac case or  $E_0/E_1 = 1/\sqrt{P}$  small. Turning specifically to Fig. 2 the solid (black) lines give the energy levels when  $E_0$  is taken to be zero, i.e.  $m \rightarrow \infty$  in the Hamiltonian Eq. (1). These straight lines as a function of  $\sqrt{B}$  are for comparison. The dashed (red) curves represent the case when a small but finite Schrödinger contribution is included in addition to the dominant Dirac contribution. It is clear that deviations between solid and dashed curves increase with  $N$  as they do with increasing  $B$ . These deviations are much more pronounced for the negative energy Landau levels as can be expected from

Fig. 1 which shows that for  $B = 0$ , the valence band has a minimum of order  $1/4\text{ eV}$  which occurs at higher values of  $k$  than is shown. This is reflected directly in the LL energies. While not seen clearly in Fig. 2 because of the restricted range of  $\sqrt{B}$  and of  $N$  shown, the negative LL index curves at large  $N$  will have a minimum at some finite value of  $\sqrt{B}$ , then increase and eventually cross the  $E = 0$  line to become positive. Note that if we expand the magnetic LL energies in lowest power of  $E_0$  we get

$$E_{N,s} = s\sqrt{2N}E_1 + E_0[N + \frac{s}{8}\frac{1}{\sqrt{2N}}\frac{E_0}{E_1}] \quad (6)$$

The leading correction is of order  $E_0$  which scales like  $B$  and hence shows a quadratic departure of the dashed (red) curve in Fig. 2 from the solid black straight lines. The coefficient of  $E_0$  in Eq. (6) is  $N$  so that these quadratic deviations increase with value of LL index  $N$ .

The DC transverse Hall conductivity  $\sigma_{xy}(\omega = 0)$  can be calculated from the LL energies of Eq. (4) but further required a knowledge of the corresponding eigen functions. Following Ref. [9] we can write

$$|N, s\rangle = \begin{bmatrix} C_{\uparrow,N,s}|N-1\rangle_{\uparrow} \\ C_{\downarrow,N,s}|N\rangle_{\downarrow} \end{bmatrix} \quad (7)$$

with  $s = +/ -$  and the coefficients  $C_{\uparrow(\downarrow),N,s}$  can be written in terms of the Diracness index  $P$  previously introduced. For  $N > 0$

$$C_{\uparrow,N,s} = \frac{\sqrt{\sqrt{1/4 + 2NP} - s/2}}{J} \\ C_{\downarrow,N,s} = \frac{-s\sqrt{\sqrt{1/4 + 2NP} + s/2}}{J} \quad (8)$$

with  $J = \sqrt{2\sqrt{1/4 + 2NP}}$ . For  $N = 0$ ,  $C_{\uparrow,0} = 0$  and  $C_{\downarrow,0} = 1$  and only  $s = +$  need be considered. The current operator  $j_\alpha$  is related to velocity  $v_x$  and  $v_y$  by

$$v_x = \frac{\hbar k_x}{m} + \frac{\alpha}{\hbar}\sigma_y \quad (9)$$

and

$$v_y = \frac{\hbar(k_y + eBx/\hbar)}{m} - \frac{\alpha}{\hbar}\sigma_x \quad (10)$$

The standard Kubo formula for the finite frequency ( $\omega$ ) optical conductivity  $\sigma_{\alpha\beta}(\omega)$  takes the form<sup>9</sup>

$$\sigma_{\alpha\beta}(\omega) = \frac{-i}{2\pi l_B^2} \sum_{N,N',s,s'} \frac{f_{N,s} - f_{N',s'}}{E_{N,s} - E_{N',s'}} \\ \times \frac{\langle N, s | j_\alpha | N', s' \rangle \langle N', s' | j_\beta | N, s \rangle}{\omega - E_{N,s} + E_{N',s'} + i/(2\tau)} \quad (11)$$

where  $1/\tau$  is a small constant residual scattering term and  $f_{N,s}$  the Fermi-Dirac distribution function given by

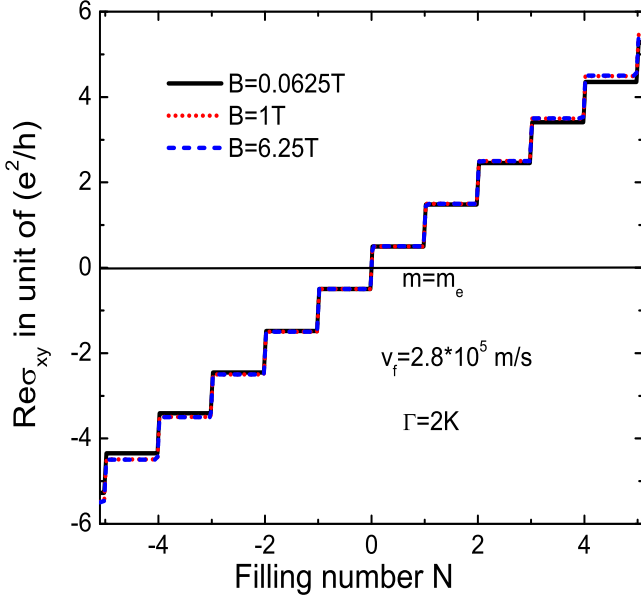


FIG. 3. (Color online) Real part of DC Hall conductivity  $Re\sigma_{xy}(\omega = 0)$  in units of  $e^2/h$  as a function of filling number  $N$  for three cases. The solid black steps apply to a small magnetic field of 0.0625 Tesla. It includes a small Schrödinger contribution to the Hamiltonian (1) with mass  $m$  equal to the free electron mass in addition to a dominant Dirac contribution with  $v_F = 2.8 \times 10^5$  m/s. It deviates only very slightly from the pure Dirac case and the quantization is  $1/2, 3/2, 5/2 \dots$  on the vertical axis. For (red) dotted curve  $B$  has been increased to 1 Tesla and for the (blue) dashed curve  $B = 6.25$  T. These curves do not deviate from Dirac quantization of the Hall plateaux.

$1/(e^{\beta(\omega-\mu)} + 1)$  with  $\beta$  the inverse temperature  $T$  and  $\mu$  the chemical potential. Defining

$$H(N, s, s') = -1 + s\sqrt{1/4 + 2NP} - s'\sqrt{1/4 + 2(N+1)P} \quad (12)$$

and

$$F(N, s, s') = \left( \frac{\sqrt{N}}{\sqrt{2}} C_{\uparrow, N+1, s'}^* C_{\uparrow, N, s} + \frac{\sqrt{N+1}}{\sqrt{2}} \times C_{\downarrow, N+1, s'}^* C_{\downarrow, N, s} - \sqrt{P} C_{\uparrow, N+1, s'}^* C_{\downarrow, N, s} \right)^2 \quad (13)$$

for  $N \neq 0$  and for  $N = 0$

$$H(0, s) = -1/2 - s\sqrt{1/4 + 2P} \quad (14)$$

$$F(0, s) = \left( \frac{1}{\sqrt{2}} C_{\downarrow, 1, s} - \sqrt{P} C_{\uparrow, 1, s} \right)^2 \quad (15)$$

the Kubo formula (11) for the DC limit of the Hall

conductivity  $\sigma_{xy}(\omega)$  reduces to

$$Re\sigma_{xy} = \frac{e^2}{h} \left\{ \sum_{N=1, s, s'} \left[ \tanh \frac{(E_{N+1, s'} - \mu)}{2T} - \tanh \frac{(E_{N, s} - \mu)}{2T} \right] \frac{F(N, s, s')}{H^2(N, s, s')} + \sum_s \frac{F(0, s)}{H^2(0, s)} \right. \\ \left. \times \left[ \tanh \frac{(E_{1, s} - \mu)}{2T} - \tanh \frac{(E_{0, +} - \mu)}{2T} \right] \right\} \quad (16)$$

In these expressions  $F(N, s, s')$  and  $H(N, s, s')$  involve the wave functions associated with the Hamiltonian (3) with  $F$  and  $H$  given by Eq. (12,13,14,15). Here we refer to the combination  $F/H^2$  as the optical matrix element (OME).

### III. DC HALL CONDUCTIVITY IN THE DIRAC LIMIT AND SCHRÖDINGER LIMIT

In the pure Dirac limit there is no mass term,  $P \rightarrow \infty$ , we have

$$H(N, s, s') = s\sqrt{2NP} - s'\sqrt{2(N+1)P} \\ F(N, s, s') = (-\sqrt{P} C_{\uparrow, N+1, s'}^* C_{\downarrow, N, s})^2 \quad (17)$$

$$C_{\uparrow, N, s} \approx \frac{1}{\sqrt{2}}, C_{\downarrow, N, s} \approx \frac{s}{\sqrt{2}} \quad (18)$$

for  $N \neq 0$  and for  $N = 0$

$$H(0, s) = -s\sqrt{2P}, F(0, s) = \left( -\frac{\sqrt{P}}{\sqrt{2}} \right)^2 \quad (19)$$

Thus the DC Hall conductivity becomes

$$Re\sigma_{xy}(\omega) = \frac{e^2}{4h} \left\{ \sum_{N=1, s, s'} \frac{(\tanh \frac{(E_{N+1, s'} - \mu)}{2T} - \tanh \frac{(E_{N, s} - \mu)}{2T})}{(s\sqrt{2N} - s'\sqrt{2(N+1)})^2} \right. \\ \left. + \sum_s (\tanh \frac{(E_{1, s} - \mu)}{2T} - \tanh \frac{(E_{0, +} - \mu)}{2T}) \right\} \\ = \frac{e^2}{4h} \left\{ -2 \tanh \frac{(E_{0, +} - \mu)}{2T} + \sum_{N=1} [\tanh \frac{(E_{N, +} - \mu)}{2T} + \tanh \frac{(E_{N, -} - \mu)}{2T}] L(N) \right\} \quad (20)$$

where  $L(N) = \frac{1}{(\sqrt{2N} - \sqrt{2(N-1)})^2} - \frac{1}{(\sqrt{2N} - \sqrt{2(N+1)})^2} + \frac{1}{(\sqrt{2N} + \sqrt{2(N-1)})^2} - \frac{1}{(\sqrt{2N} + \sqrt{2(N+1)})^2} = -2$ . So we recover the well known result<sup>26</sup> which applies to pure relativistic Dirac fermions

$$Re\sigma_{xy} = \frac{e^2}{h} \left\{ \frac{1}{2} \tanh \frac{\mu}{2T} + \frac{1}{2} \times \sum_{N=1} [\tanh \frac{(\mu - E_{D, N})}{2T} + \tanh \frac{(\mu + E_{D, N})}{2T}] \right\} \quad (21)$$

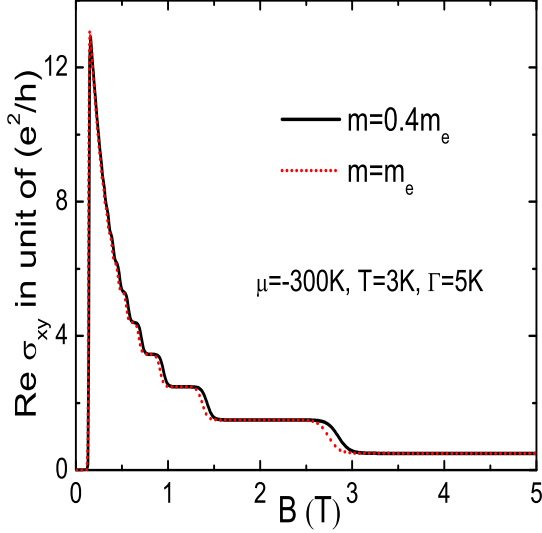


FIG. 4. (Color online) Real part of DC Hall conductivity  $Re\sigma_{xy}(\omega = 0)$  in units of  $e^2/h$  as a function of magnetic field  $B$  in Tesla. The chemical potential is  $\mu = -300K$ , the temperature  $T = 3K$  and the residual scattering rate in Eq. (11) is set at  $\Gamma = 5K = 1/(2\tau)$ . The sign of the Hall conductivity by our definition is negative for  $\mu = -300K$ , only in this figure do we change the sign to be positive. The dotted (red) curve are results for the mass  $m = m_e$  (free electron mass) and the solid black for  $m = 0.4m_e$  which increases the effect of the Schrödinger term in the Hamiltonian (1).

where  $E_{D,N} = \sqrt{2N\alpha^2/l_B^2}$ . This expression appears as Eq. (6) in the paper of Gusynin and Sharapov<sup>26</sup> and gives the quantization series  $1/2, 3/2, 5/2, \dots$ . In the pure Schrödinger limit,  $P = 0$ , we have

$$H(N, s, s') = -1$$

$$F(N, s, s') = \left(\frac{\sqrt{N+1}}{\sqrt{2}}\right)^2 = \frac{N+1}{2} \quad (22)$$

so the DC Hall conductivity becomes

$$Re\sigma_{xy} = \frac{e^2}{h} \sum_{N=0} \left[ \left( \tanh \frac{(E_{S,N+1} - \mu)}{2T} - \tanh \frac{(E_{S,N} - \mu)}{2T} \right) (N+1) \right] \quad (23)$$

where  $E_{S,N} = \hbar^2(N + \frac{1}{2})/(ml_B^2)$ . This is the standard expression for the classical Schrödinger case, and gives the usual quantization  $0, 1, 2, 3, \dots$  as discussed in Ref. [26].

#### IV. NUMERICAL RESULTS

While we have just seen that our general expression for the integer quantum Hall effect properly reduces to the well known results for relativistic and classical electrons

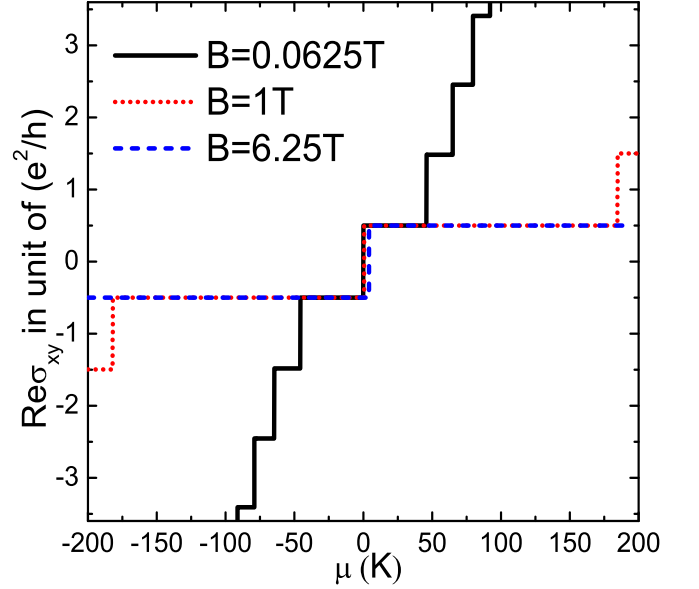


FIG. 5. (Color online) Real part of DC Hall conductivity  $Re\sigma_{xy}(\omega = 0)$  in units of  $e^2/h$  as a function of chemical potential  $(\mu)$  in units of degree  $K$ . Here  $v_F = 2.8 \times 10^5$  m/s and  $m = m_e$ . Three values of magnetic field  $B$  are considered, solid (black) curve,  $B = 0.0625$  Tesla, dotted (red) curve,  $B = 1$  Tesla and short dashed (blue) curve  $B = 6.25$  Tesla. In contrast to Fig. 3 where the horizontal axis is filling number and the steps occur at multiples of one, there is now no quantization on  $\mu$  associated with the various steps.

in the appropriate limits namely  $P = \infty$  and  $P = 0$  respectively, what we are mainly interested in here, is the case of  $1/P \ll 1$ . We want to obtain a first correction to pure Dirac i.e. a first correction in an expansion in powers of  $1/P$ . In the appendix we show how this can be done. The first formula Eq. (A1) applies to any finite  $P$  case and is the start of our analytic work which ends with Eq. (A8). This simple analytic formula gives exactly the same results as does Eq. (A1) provided  $x = 1/P$  is small ( $x \ll 1$ ). Note that the lowest power in  $x$  to appear in Eq. (A2) to Eq. (A7) which give the corrections to the optical matrix elements, is  $\sqrt{x}$  rather than  $x$ . By definition  $\sqrt{x} = E_0/E_1 = \frac{\hbar}{mv_F} \sqrt{e|B|/\hbar}$ . This quantity can be small for three reasons,  $m$  can be made large which is equivalent to having a very small Schrödinger term in the Hamiltonian Eq. (1). The velocity  $v_F$  large, also makes  $\sqrt{x}$  small as it corresponds to increasing the importance of the Dirac term. Finally for fix  $m$  and  $v_F$ ,  $\sqrt{x}$  can still be made small by making the magnetic field small. For the range of parameters used in this work the deviations from pure Dirac behavior of the relativistic integer quantum Hall effect is negligible except at small  $B$  as we see in Fig. 3. The solid black curve corresponds to a rather small value of magnetic field  $B = 0.0625T$  for which  $\sqrt{x} = 1/\sqrt{P} = 0.0027$ . The curve shows very small deviations from the pure Dirac case as given for

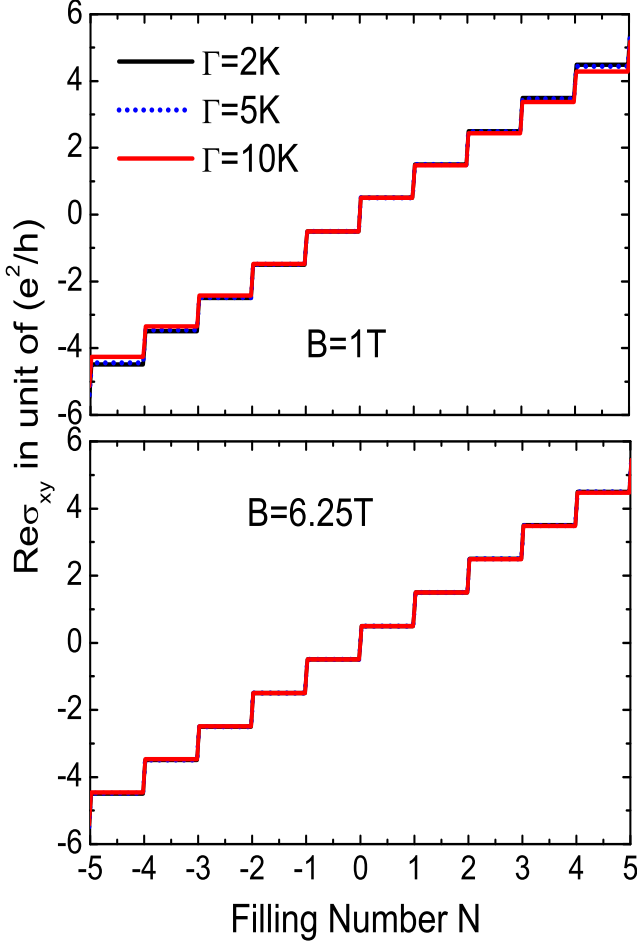


FIG. 6. (Color online) Real part of DC Hall conductivity  $\text{Re}\sigma_{xy}(\omega=0)$  in units of  $e^2/h$  as a function of filling number  $N$  for magnetic field  $B=1$  Tesla (top frame) and  $B=6.25$  Tesla (bottom frame). Here  $v_F=2.8 \times 10^5$  m/s and  $m=m_e$ . The solid black curve is for the residual scattering rate in Eq. (11)  $\Gamma=1/(2\tau)=2\text{K}$ , dotted blue for  $5\text{K}$  and solid red for  $10\text{K}$ . At the smaller value of  $B$  (upper frame) small differences in the heights of the plateaux can be seen. These vanish as  $B$  is increased (lower frame).

example in Refs. [25,26]. Here we remind the reader that the parameters chosen as representative of a topological insulator were  $v_F=2.8 \times 10^5$  m/s and  $m=m_e$  (the bare electron mass) and the scattering rate  $\Gamma=1/(2\tau)=2\text{K}$  in Eq. (11). It is this  $\Gamma$  which is responsible for the small changes of the black curve from relativistic quantization which would certainly apply in the clean limit where the Landau levels remain individually well defined even for small values of the magnetic field  $B$ . If  $B$  is increased to  $B=1\text{T}$  (Tesla) which corresponds to a  $\sqrt{x}$  value of 0.011, the red dotted curve is exactly the pure Dirac curve as is the blue dashed curve for  $B=6.25\text{T}$ .

While formula Eq. (A1) is generally valid, it is hard to use because it requires knowledge of  $H(N, s, s')$ ,

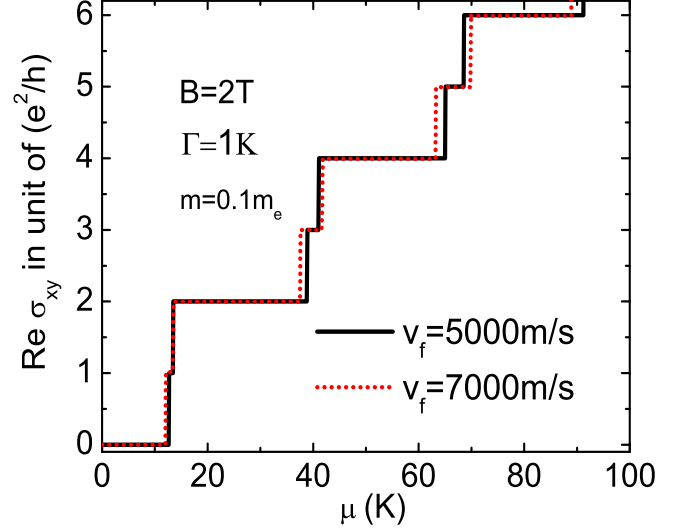


FIG. 7. (Color online) Real part of DC Hall conductivity  $\text{Re}\sigma_{xy}(\omega=0)$  in units of  $e^2/h$  as a function of chemical potential  $\mu$  for magnetic field  $B=2$  Tesla. The parameters used<sup>30</sup> are typical for spintronic semiconductors with Rashba spin orbit coupling, and are the same as for Fig. 1b.

$F(N, s, s')$  and  $H(0, s)$ ,  $F(0, s)$  of formulas Eq. (12) to Eq. (15) respectively. By contrast the final but approximate formula obtained in appendix A

$$\text{Re}\sigma_{xy} = \frac{e^2}{h} \left\{ \frac{1}{2} \tanh \frac{(\mu - E_{0,+})}{2T} + \frac{1}{2} \times \sum_{N=1} [\tanh \frac{(\mu - E_{N,+})}{2T} + \tanh \frac{(\mu - E_{N,-})}{2T}] \right\} \quad (24)$$

can be evaluated directly from a knowledge of  $\mu$  (the chemical potential) and the energies of the LL  $E_{N,s}$ . There are no corrections in this equation coming from the optical matrix elements (A2) to (A7). These were expanded to order  $x^{3/2}$  and found to cancel out entirely. What could provide deviations of the Hall plateaux from the pure relativistic Dirac prediction are terms in Eq. (24) proportional to  $\sqrt{x}$  and  $x$ , and higher orders that appear in the energies. But these appear in the tanh's which at zero temperature are just step functions one or zero and consequently this does not change the height of the Hall plateaux as we next further emphasize. However it does change the value of the chemical potential at which the jumps occur.

In Fig. 4 we show our results for the DC Hall conductivity  $\text{Re}\sigma_{xy}(\omega=0)$  in units of  $e^2/h$  as a function of magnetic field  $B$  in Tesla for fixed value of chemical potential. We have chosen the other parameters to correspond to those used in Fig.3a of Ref. [25] where the case of graphene was discussed and this serves as a test of the accuracy of our work. The chemical potential is  $\mu=-300\text{K}$ , the temperature  $T=3\text{K}$ , the residual scat-

tering rate  $\Gamma = 5K$ . The dotted curve (red) includes an effective mass ( $m$ ) equal to the free electron mass ( $m_e$ ) and the solid (black) curve has  $m = 0.4m_e$  which implies a relatively larger Schrödinger contribution and consequently larger deviations from a pure Dirac case. Accounting for a degeneracy factor of 4 (spin and valley) used in Ref. [25] and not in our work, our results agree with those presented in their Fig.3a when we consider pure graphene. As we expect, there are however small deviations between our results and those of Ref. [25] which become more noticeable as  $m$  decreases. It is important to compare carefully the results of Fig. 4 with those of Fig. 3. In Fig. 4 we have kept the chemical potential fixed at a value of  $\mu = -300K$  and varied  $B$ . The step seen in the dotted curve around  $B \approx 3$  Tesla corresponds to the case when the  $N = 0$  LL is about to cross through the chemical potential and so this corresponds to the first step in Fig. 3 rather than to a large filling  $N$  value. We emphasize that there is no change in the quantization of  $\sigma_{xy}(\omega = 0)$  from the pure Dirac case but there is a change in the value of  $B$  where the steps occur and this is largest at large  $B$ . As an example we see a shift of 4% in the first step which is reduced to 2.6% in the second step (smaller  $B$  value). Finally the impurity scattering embodied in  $\Gamma$  and finite temperature has smeared out the steps between plateaux as we expect. Also, the range of  $B$  over which a given plateau manifests is greatly reduced as  $B$  is reduced. This is to be contrasted with the results in Fig. 3 where the distance between plateaux along the horizontal axis is uniform.

If instead of the filling number we had used the chemical potential for the horizontal axis as we show in Fig. 5, we no longer get equal distance steps. For the smallest value of  $B = 0.0625$  T solid (black) curve the steps from one plateau to the next are narrow and become even narrower as  $\mu$  increases because the spacing in energy between LL decreases with increasing energy. But this spacing also increases with increasing  $B$  as can be seen in the dotted (red) curve for  $B = 1$  Tesla and the dashed (blue) curve for  $B = 6.25$  Tesla. For this last curve the second step falls outside the range of  $\mu$  shown in the diagram. Another point to be made, which is seen most clearly in this last curve, is that the first step when the Hall conductivity goes from  $-1/2$  to  $1/2$  no longer occurs exactly at zero value of chemical potential but is rather at  $\mu = E_{N=0} = \hbar^2/2ml_B^2$ . This is a characteristic difference between pure Dirac and a TI. This important feature is lost in Fig.3 where filling number is used instead of the chemical potential on the horizontal axis. Finally in Fig. 6 we show results for three values of residual scattering namely  $\Gamma = 2K$  solid (black),  $\Gamma = 5K$  dashed (blue) and  $\Gamma = 10K$  solid (red). The top frame is for  $B = 1$  Tesla the bottom for  $B = 6.25$  Tesla. In all cases we see only a small effect of  $\Gamma$  on the quantization which increases slightly with increasing filling number and decreases with increasing value of  $B$ .

It is also of interest to consider the opposite limit when the dominant magnetic energy comes from the

Schrödinger term in (1) and the Dirac contribution provides a small correction. In that limit the appropriate expansion parameters is  $P = (E_1/E_0)^2$ , and the general formula (A1) is to be expanded in powers of  $P$  with  $P \ll 1$ . For  $P = 0$  we have already seen that it reduces to the classical non relativistic case. Keeping a first correction to account for a small Dirac contribution in (1) we obtain

$$\begin{aligned} Re\sigma_{xy} &= \frac{e^2}{h} \left\{ \sum_{N=0} [\tanh \frac{(E_{N+1,+} - \mu)}{2T} - \tanh \frac{(E_{N,+} - \mu)}{2T}] \right. \\ &\quad \times [\frac{1+N}{2} - (1+N)P + 6(1+N)^2P^2] \\ &\quad + \sum_{N=1} [\tanh \frac{(E_{N+1,-} - \mu)}{2T} - \tanh \frac{(E_{N,-} - \mu)}{2T}] \\ &\quad \times [\frac{N}{2} + NP - 6N^2P^2] \\ &\quad + \sum_{N=0} [\tanh \frac{(E_{N+1,-} - \mu)}{2T} - \tanh \frac{(E_{N,+} - \mu)}{2T}] \\ &\quad \left. \times [P - 6(1+2N)P^2] \right\} \end{aligned} \quad (25)$$

This equation contains powers of  $P$  and  $P^2$  terms from the expansion of the optical matrix elements. However as we will see below these terms drop out of the final formula (27). This means that corrections to the classical case coming from the OME are very small and must be of higher order than  $(E_1/E_0)^4$ . This is to be contrasted with the case applicable for topological insulators where we found that the correction to the pure relativistic case must be of higher order than cubic in  $E_1/E_0$ .

To understand better the meaning of Eq. (25) in the limit  $P \ll 1$  we begin by expanding the LL energies of Eq. (4) in powers of  $P$ , we get for  $N \neq 0$ ,

$$E_{N,s} = E_0(N + s/2) + s2N(E_1/E_0)^2 E_0 \quad (26)$$

and  $E_{N=0}$  retains the form it has in Eq. (5). If first we neglect the  $(E_1/E_0)^2$  correction in Eq. (26) we see that for positive  $s$ ,  $E_0$  plus the sequence  $N = 1, 2, \dots$  give the classical result for the LL series and for negative  $s$ ,  $N = 1, 2, \dots$  give a second such sequence. Thus we have two LL sequences which accounts for spin degeneracy. When  $(E_1/E_0)^2 \ll 1$  the negative  $s$  sequence is slightly shifted down and the positive  $s$  sequence is shifted up by the same amount and  $E_{N+1,-} = E_{N,+} - 2(2NE_0P)$ . The two sequence involved can be reorganized to get

$$\begin{aligned} Re\sigma_{xy} &= \frac{e^2}{h} \left\{ \sum_{N=0} [\tanh \frac{(E_{N+1,+} - \mu)}{2T} - \tanh \frac{(E_{N,+} - \mu)}{2T}] \right. \\ &\quad \times (1+N)/2 + \sum_{N=1} [\tanh \frac{(E_{N+1,-} - \mu)}{2T} \\ &\quad \left. - \tanh \frac{(E_{N,-} - \mu)}{2T}] \times \frac{N}{2} \right\} \end{aligned} \quad (27)$$

This is a second important result of this work.

In Fig. 7 we show results for the DC Hall conductivity as a function of chemical potential  $\mu$  for parameters typical of present day spintronic semiconductors.<sup>30</sup> The Schrödinger mass  $m$  in Eq. (1) is set at ( $m = 0.1m_e$ ) one tenth of the bare electron mass and two values of Dirac velocities namely  $v_F = 5000m/s$  (solid black curve) and  $v_F = 7000m/s$  (dotted red) are considered. The residual scattering rate  $\Gamma = 1K$  and the magnetic field is  $B = 2T$  for both cases. Even though we have taken values of the Dirac velocity which are near their maximum in spintronic semiconductors,<sup>30</sup> we see that the deviations from the classical case are small. The quantization remains classical but two such series are involved which are slightly shift with the shift between the two increasing with increasing  $\mu$  as we expect from Eq. (26).

## V. SUMMARY AND CONCLUSIONS

The helical electrons which exist at the surface of topological insulators have electronic dispersion curves which include a subdominant Schrödinger quadratic in momentum part characterized by an effective mass  $m$  and a dominant Dirac linear in momentum part described by a Fermi velocity  $v_F$ . The small quadratic piece distorts the usual Dirac cones of graphene and gives them instead an hourglass shape and is responsible for particle-hole asymmetry. In a magnetic field oriented perpendicular to the plane of the helical surface electrons, Landau levels form but these require a much more complicated mathematical description than when either Schrödinger or Dirac term is present separately. We have derived formulas for the DC Hall conductivity that cover the mixed case and which are valid for any value of Schrödinger and Dirac energy scale,  $E_0 = \hbar e|B|/m$  and  $E_1 = \alpha\sqrt{e|B|/\hbar}$  respectively. In general our formulas need to be evaluated numerically, as the matrix elements of the current now do not have a simple form. The Landau level energies are also complicated expressions of the LL index  $N$ . In the limit  $E_0 = 0$ ,  $\sigma_{xy}(\omega = 0)$  reduces to the known quantized Hall plateaux  $1/2, 3/2, 5/2...$  (Dirac) in units of  $e^2/h$  while for  $E_1 = 0$  the plateaux are at  $0, 1, 2, 3...$  (Schrödinger).

We have also reduced our general expressions to a much simpler form in the limit when  $E_0$  can be considered to be a small perturbation on the pure Dirac case. This is the case of greatest interest in this paper. To accomplish this we expanded the optical matrix elements to second order of perturbation theory in powers of  $\sqrt{x} = (E_0/E_1)$ .

This leads to a simple formula for  $Re\sigma_{xy}(\omega = 0)$  which depends only on the Landau level energies  $E_{N,s}$  with  $s = \pm 1$ , given by Eq. (4) and Eq. (5), and on the chemical potential ( $\mu$ ). The parameter  $x$  coming from the expansion of the optical matrix element dropped out entirely. This formula is given by Eq. (24) which is one of our important results. It has the same form as for the pure Dirac case except that it is the Landau level energies of the TI which appear in the thermal factors and these contain a contribution from the subdominant Schrödinger term in the Hamiltonian (1). The Hall plateaux however keep their relativistic quantization even though  $x$  is not zero, and the value of chemical potential at which the hall conductivity jumps from a negative to a positive value is no longer zero but is at  $\mu = E_0/2$ .

The central parameter  $\sqrt{x} = E_0/E_1 = \sqrt{e|B|/\hbar}/(mv_F)$  can be small for three reasons. The magnetic field can be made small, or the Schrödinger mass  $m$  or the Dirac Fermi velocity ( $v_F$ ) can be made large. A large mass means a small quadratic term in our Hamiltonian (1) and a large  $v_F$  means a large Dirac contribution. Our numerical work based on the exact equations for the DC Hall plateaux confirms that for a large range of  $x$ , we indeed recover the pure Dirac quantization pattern as our Eq. (24) predicts. These results are of interest within the context of presently discovered topological insulators. We have also considered the opposite limit when the Schrödinger term dominates and the Dirac term is a small correction. In this case the appropriate expansion of the optical matrix elements which appear in our general formula is to consider powers of  $E_1/E_0$ . Working to order  $(E_1/E_0)^4$  we find a complete cancelation of these factors in the optical matrix elements and we are left with the classical quantization series for the Hall plateaux split however into two series with splitting related to shifts in the Landau levels energies brought about by the subdominant spin orbit coupling. This is another of our important results and is relevant to present day spintronic semiconductors.

## ACKNOWLEDGMENTS

This work was supported by the Natural Sciences and Engineering Research Council of Canada (NSERC) and the Canadian Institute for Advanced Research (CIFAR).

## REFERENCES

\* lizhou@mcmaster.ca

† carbotte@mcmaster.ca

<sup>1</sup> M. Z. Hasan and C. L. Kane, Rev. Mod. Phys. **82**, 3045 (2010).

<sup>2</sup> X.-L. Qi and S.-C. Zhang, Rev. Mod. Phys. **83**, 1057 (2011).

<sup>3</sup> Y. L. Chen, J.-H. Chu et.al, Science **329**, 659(2010).

<sup>4</sup> S.-Y. Xu, X Xia et.al, Science **332**, 560 (2011).



- <sup>5</sup> Y. L. Chen, J. G. Analytis et.al, Science **325**, 178(2009).
- <sup>6</sup> D. Hsieh et.al, Nature (London), **460**, 1101 (2009).
- <sup>7</sup> J. N. Hancock, et.al, Phys. Rev. Lett. **107**, 136803(2011).
- <sup>8</sup> Zhou Li and J. P. Carbotte, Phys. Rev. B **87**, 155416 (2013).
- <sup>9</sup> Zhou Li and J. P. Carbotte, Phys. Rev. B **88**, 045414 (2013).
- <sup>10</sup> Zhou Li, F. Marsiglio and J. P. Carbotte, Scientific Reports **3**, 2828 (2013).
- <sup>11</sup> A. R. Wright and R. H. McKenzie, Phys. Rev. B **87**, 085411 (2013).
- <sup>12</sup> J.N. Fuchs, F. Piechon, M.O. Goerbig and G. Montambaux, Eur. Phys. J. B **77**, 351 (2010).
- <sup>13</sup> A. R. Wright, Phys. Rev. B **87**, 085426 (2013).
- <sup>14</sup> A. A. Taskin and Y. Ando, Phys. Rev. B **84**, 035301 (2011).
- <sup>15</sup> G. P. Mikitik and Yu. V. Sharlai, Phys. Rev. B **85**, 033301 (2012).
- <sup>16</sup> T. Champel and V. P. Mimsev, Philos. Mag. B **81**, 55 (2001).
- <sup>17</sup> Igor A. Luk'yanchuk and Yakov Kopelevich, Phys. Rev. Lett. **93**, 166402 (2004).
- <sup>18</sup> S. G. Sharapov, V. P. Gusynin and H. Beck, Phys. Rev. B **69**, 075104 (2004).
- <sup>19</sup> V. P. Gusynin and S. G. Sharapov, Phys. Rev. B **71**, 125124 (2005).
- <sup>20</sup> Z. Wang, Z.-G. Fu, S.-X. Wang and Ping Zhang, Phys. Rev. B **82**, 085429 (2010).
- <sup>21</sup> V. P. Gusynin, S. G. Sharapov and J. P. Carbotte, J. Phys: Condensed matter **19**, 026222 (2007).
- <sup>22</sup> A. Pound, J. P. Carbotte and E. J. Nicol, Phys. Rev. B **85**, 125422 (2012).
- <sup>23</sup> C. J. Tabert and E. J. Nicol, Phys. Rev. Lett. **110**, 197402 (2013).
- <sup>24</sup> F. D. M. Haldane, Phys. Rev. Lett. **61**, 2015 (1988).
- <sup>25</sup> V. P. Gusynin and S. G. Sharapov, Phys. Rev. B **73**, 245411 (2006).
- <sup>26</sup> V. P. Gusynin and S. G. Sharapov, Phys. Rev. Lett **95**, 146801 (2005).
- <sup>27</sup> K. S. Novoselov et.al, Nature **438**, 197 (2005).
- <sup>28</sup> X. Zhang, Y.-W. Tan, H. L. Stormer and P. Kim, Nature **438**, 201 (2005).
- <sup>29</sup> C.-X. Liu, X.-L. Qi, H. J. Zhang, X. Dai, Z. Fang and S.-C. Zhang, Phys. Rev. B **82**, 045122 (2010).
- <sup>30</sup> J. Fabian, A. Matos-Abiague, C. Ertler, P. Stano and I. Žutić, Acta Physica Slovaca **57**, No. 4 and 5, 565 (2007)

## Appendix A: Derivation of the DC hall conductivity for the topological insulator

With the mass term included the Hall conductivity is given by

$$\begin{aligned}
 Re\sigma_{xy} = & \frac{e^2}{h} \left\{ \sum_{N=1} \left[ \left( \tanh \frac{(E_{N+1,+} - \mu)}{2T} \right. \right. \right. \\
 & - \tanh \frac{(E_{N,+} - \mu)}{2T} \left. \right) \frac{F(N, +, +)}{H^2(N, +, +)} \\
 & + \left( \tanh \frac{(E_{N+1,+} - \mu)}{2T} - \tanh \frac{(E_{N,-} - \mu)}{2T} \right) \frac{F(N, -, +)}{H^2(N, -, +)} \\
 & + \left( \tanh \frac{(E_{N+1,-} - \mu)}{2T} - \tanh \frac{(E_{N,+} - \mu)}{2T} \right) \frac{F(N, +, -)}{H^2(N, +, -)} \\
 & + \left. \left( \tanh \frac{(E_{N+1,-} - \mu)}{2T} - \tanh \frac{(E_{N,-} - \mu)}{2T} \right) \frac{F(N, -, -)}{H^2(N, -, -)} \right] \\
 & + \sum_s \left( \tanh \frac{(E_{1,s} - \mu)}{2T} - \tanh \frac{(E_{0,+} - \mu)}{2T} \right) \frac{F(0, s)}{H^2(0, s)} \Big\} \quad (A1)
 \end{aligned}$$

In a general case Eq. (A1) is complicated, although it is explicit, because the Landau level energies are not simple functions of the LL index  $N$  and more importantly the current matrix elements are particularly long algebraic expressions. After expanding the OME in power of  $x = 1/P$  and retaining terms to the order of  $x^{3/2}$  only, we obtained

$$\begin{aligned}
 \frac{F(N, +, +)}{H^2(N, +, +)} = & \frac{1}{8(\sqrt{N} - \sqrt{1+N})^2} \\
 & + \frac{(1/\sqrt{N} + 1/\sqrt{N+1})\sqrt{x}}{16\sqrt{2}} \\
 & - \frac{(1/\sqrt{N^3} + 1/\sqrt{(N+1)^3})x^{3/2}}{256\sqrt{2}}, \quad (A2)
 \end{aligned}$$

$$\begin{aligned}
 \frac{F(N, -, +)}{H^2(N, -, +)} = & \frac{1}{8(\sqrt{N} + \sqrt{1+N})^2} \\
 & - \frac{(1/\sqrt{N} - 1/\sqrt{N+1})\sqrt{x}}{16\sqrt{2}} \\
 & + \frac{(1/\sqrt{N^3} - 1/\sqrt{(N+1)^3})x^{3/2}}{256\sqrt{2}}, \quad (A3)
 \end{aligned}$$

$$\begin{aligned}
 \frac{F(N, +, -)}{H^2(N, +, -)} = & \frac{1}{8(\sqrt{N} + \sqrt{1+N})^2} \\
 & + \frac{(1/\sqrt{N} - 1/\sqrt{N+1})\sqrt{x}}{16\sqrt{2}} \\
 & - \frac{(1/\sqrt{N^3} - 1/\sqrt{(N+1)^3})x^{3/2}}{256\sqrt{2}} \quad (A4)
 \end{aligned}$$

$$\begin{aligned}
\frac{F(N, -, -)}{H^2(N, -, -)} &= \frac{1}{8(\sqrt{N} - \sqrt{1+N})^2} \\
&- \frac{(1/\sqrt{N} + 1/\sqrt{N+1})\sqrt{x}}{16\sqrt{2}} \\
&+ \frac{(1/\sqrt{N^3} + 1/\sqrt{(N+1)^3})x^{3/2}}{256\sqrt{2}}
\end{aligned} \tag{A5}$$

and

$$\frac{F(0, +)}{H^2(0, +)} = \frac{1}{4} + \frac{\sqrt{x}}{8\sqrt{2}} - \frac{x^{3/2}}{128\sqrt{2}} \tag{A6}$$

$$\frac{F(0, -)}{H^2(0, -)} = \frac{1}{4} - \frac{\sqrt{x}}{8\sqrt{2}} + \frac{x^{3/2}}{128\sqrt{2}} \tag{A7}$$

Substituting this into Eq. (A1) leads to the approximate expression for the Hall conductivity

$$\begin{aligned}
Re\sigma_{xy} &= \frac{e^2}{h} \left\{ \frac{1}{2} \tanh \frac{(\mu - E_{0,+})}{2T} + \frac{1}{2} \times \right. \\
&\left. \sum_{N=1} [\tanh \frac{(\mu - E_{N,+})}{2T} + \tanh \frac{(\mu - E_{N,-})}{2T}] \right\}
\end{aligned} \tag{A8}$$

which is a central results of this work. It provides a simple compact analytic formula for the DC Hall conductivity of a topological insulator which includes a first correction to a dominant Dirac Hamiltonian with an additional small subdominant Schrödinger part i.e. a small piece quadratic in momentum. In mathematical term we have made an expansion of the optical matrix elements of Eq. (A1), which is itself valid for any value of Schrödinger and Dirac, in power of  $x = 1/P$  where  $P$  is the Diracness defined as  $E_1^2/E_0^2$ . Here  $E_0 = \hbar e|B|/m$  and  $E_1 = \alpha\sqrt{e|B|/\hbar}$ . This first energy  $E_0$  determines the Landau levels for a pure Schrödinger (classical) case while  $E_1$  is the magnetic energy associated with the LL for a pure Dirac (relativistic) spectrum. All optical matrix element corrections have dropped out to order  $x^{3/2}$ . Equation (A8) differs from (21) for pure Dirac only through the appearance of the energies  $E_{0,+}$ ,  $E_{N,+}$  and  $E_{N,-}$  which here include a small Schrödinger piece. However at zero temperature the tanh factors in (A8) are just step functions which are either zero or one as before but with the chemical potential value at which these jumps occur modified by the Schrödinger contribution to the energies.